Magnetic Resonance in Medicine 66:1079–1088 (2011)

In Vivo Noninvasive 4D Pressure Difference Mapping in the Human Aorta: Phantom Comparison and Application in Healthy Volunteers and Patients

Jelena Bock,[1]* Alex Frydrychowicz,[2] Ramona Lorenz,[1] Daniel Hirtler,[3] Alex J. Barker,[1] Kevin M. Johnson,[2] Raoul Arnold,[3] Hans Burkhardt,[4] Juergen Hennig,[1] and Michael Markl[1]

In this work, we present a systematic phantom comparison and clinical application of noninvasive pressure difference mapping in the human aorta based on time-resolved 3D phase contrast data. Relative pressure differences were calculated based on integration and iterative refinement of pressure gradients derived from MR-based three-directional velocity vector fields (flow-sensitive 4D MRI with spatial/temporal resolution ~ 2.1 mm^3/40 ms) using the Navier-Stokes equation. After in vitro study using a stenosis phantom, time-resolved 3D pressure gradients were systematically evaluated in the thoracic aorta in a group of 12 healthy subjects and 6 patients after repair for aortic coarctation. Results from the phantom study showed good agreement with expected values and standard methods (Bernoulli). Data of healthy subjects showed good intersubject consistency and good agreement with the literature. In patients, pressure waveforms showed elevated peak values. Pressure gradients across the stenosis were compared with reference measurements from Doppler ultrasound. The MRI findings demonstrated a significant correlation ($r = 0.96$, $P < 0.05$) but moderate underestimation (14.7% ± 15.5%) compared with ultrasound when the maximum pressure difference for all possible paths connecting proximal and distal locations of the stenosis were used. This study demonstrates the potential of the applied approach to derive additional quantitative information such as pressure gradients from time-resolved 3D phase contrast MRI. Magn Reson Med 66:1079–1088, 2011. © 2011 Wiley-Liss, Inc.

Key words: flow sensitive PC-MRI; blood pressure gradients; aorta; hemodynamic; relative pressure difference

Pressure gradients are an important clinical marker for the severity of cardiovascular disease such as aortic valve stenosis and aortic coarctation (1,2). In the clinical routine, catheter measurements are considered the gold standard to determine the pressure gradients in vivo. Although this method is reported to be reliable and of low risk (3,4), it remains an invasive procedure with its associated potential risk of severe side-effects and involves radiation exposure for catheter guidance. Alternatively, pressure gradient Δp can also be estimated using the simplified Bernoulli equation [$\Delta p = 4V_{max}^2$] (5–7) based on maximum velocity V_{max} measurements as derived from clinical standard Doppler ultrasound (US). However, V_{max} measures with ultrasound are operator dependent and subject to errors from poor acoustic windows and spectral broadening. Pressure difference (PD) estimation is highly sensitive to velocity measurements errors of V_{max} due to the exponentiation of velocities in the Bernoulli equation.

Furthermore, the simplified Bernoulli equation neglects important boundary conditions such as the velocity proximal to the coarctation and the shape of the stenosis as discussed in detail by Oshinski et al. (7). Although the immediate output of the Bernoulli equation is useful to obtain a value representing hemodynamic pressure drops in region of interest, it does not easily provide information regarding temporal and spatial variations across the stenosis.

Alternatively, it is possible to noninvasively and without user-dependency derive relative pressure gradients by using the time-resolved velocity field measured with noninvasive and user independent time-resolved (CINE) three-directionally encoded phase contrast (PC) MRI. Pressure gradients can be calculated by solving the Navier-Stokes equation (8–10) assuming blood as an incompressible, laminar Newtonian fluid. Unlike simplified Bernoulli, this approach apparently offers the advantage to estimate temporally and spatially distributed pressure gradients within a vessel segment. Subsequent spatial integration and iterative refinement can be used to derive time-resolved PD maps as reported by Tyszka et al. (9) and Ebbers et al. (10).

In recent animal studies, 3D PD mapping based on radial time-resolved 3D PC-MRI has been applied in different vascular regions and reported to be stable and robust (11,12). However, previous human studies relied either on data from 2D slices (8), calculated pressure

[1]Department of Radiology, Medical Physics, University Medical Center Freiburg, Freiburg, Germany.
[2]Department of Radiology, University of Wisconsin-Madison, Madison, Wisconsin, USA.
[3]Department of Pediatric Cardiology and Congenital Heart Disease, University Medical Center Freiburg, Freiburg, Germany.
[4]Institute for Computer Science, University of Freiburg, Freiburg, Germany.

Part of this work was presented at the ISMRM 2009 in Honolulu, USA.

Grant sponsor: Deutsche Forschungsgemeinschaft (DFG); Grant number: MA 2383/5-1; Grant sponsor: Bundesministerium für Bildung und Forschung (BMBF); Grant number: 01EV0706.

*Correspondence to: Jelena Bock, Dipl.-Ing., Department of Radiology, Medical Physics, University Medical Center Freiburg, Breisacher Strasse 60a, 79106 Freiburg, Germany. E-mail: jelena.bock@uniklinik-freiburg.de

Received 13 August 2010; revised 14 February 2011; accepted 15 February 2011.

DOI 10.1002/mrm.22907
Published online 24 March 2011 in Wiley Online Library (wileyonlinelibrary.com).

gradients only along predefined pathways (10,13) or were based on data from a single healthy volunteer (9,14). To date, no systematic in vivo study in volunteers and patients on 3D pressure gradient mapping determined from PC-MRI has been reported. Moreover, recent advances in 3D CINE PC-MRI with three-directional velocity encoding (flow sensitive 4D MRI) permit the reliable acquisition of pulsatile 3D blood flow data in the entire aorta, which is ideally suited for 3D pressure gradient estimation (15).

It was, therefore, the purpose of this study to evaluate the potential of a data analysis strategy for the assessment of spatial and temporal (4D) PDs distribution in the human aorta. In vitro experiments in a controlled environment using stenosis phantoms were performed to compare the PD mapping technique with the established simplified Bernoulli approach before a transfer to human volunteers and patients with aortic coarctation was performed.

MATERIALS AND METHODS

In Vitro Measurements

For methods' comparison, all in vitro measurements were performed using time-resolved three directionally encoded PC-MRI on a 3 T MR-System (Tim TRIO, Siemens AG, Erlangen, Germany). Blood-mimicking fluid (60% water, 40% glycerol, viscosity 4.96×10^{-3} Pa s, density 1105 kg/m^3) was used as blood substitute (16).

Measurement 1: Constant Flow

A stenosis model (pipe Ø 33.5 ± 2.0 mm, stenosis Ø 10 ± 0.1 mm) was connected to a pump (Deltastream, Medos Medizintechnik AG, Stolberg, Germany) with constant flow of 5.7 ± 0.5 L/min. Measurement parameters were: V_{enc} = 180 cm/s along all three encoding directions, spatial resolution 1.0 × 1.0 × 1.0 mm^3, field of view (FOV) = 350 × 350 mm^2, flip angle = 15°, echo time = 2.8 ms, pulse repetition time = 5.6 ms. Measurements were repeated four times with identical parameters (three times with constant flow on and once with flow off). Three flow-on-measurements were averaged to improve the signal-to-noise ratio. The flow-off-measurement was subtracted from averaged data to correct for eddy currents and Maxwell terms (17).

Measurement 2: Pulsatile Flow

A second model (pipe Ø 26.8 ± 2.0 mm, stenosis Ø 17.1 ± 0.1 mm) was connected to a pneumatically driven ventricular assist device (Medos Medizintechnik AG, Stolberg, Germany) used as pump for the generation of pulsatile flow (pump cycle = 60 ms, flow rate = 66 mL/cycle, prestenotic systolic peak velocity = 0.7 m/s) as described in detail in Ref. 18. Measurements were synchronized with the pulsatile flow cycle and acquisition parameters were: V_{enc} = 150 cm/s, spatial resolution 1.4 × 1.2 × 1.2 mm^3, temporal resolution = 42.4 ms, FOV = 350 × 284 mm^2, flip angle = 15°, echo time = 2.7 ms, pulse repetition time = 5.3 ms. Measurement was repeated once with identical parameters but with flow off. This measurement was subtracted for correction.

In Vivo Measurements

Twelve healthy subjects (mean age 24.5 ± 3.2 years, four female) and six patients after aortic coarctation repair (mean age 23.5 ± 7.3 years, two female) were included in our study after approval by the local ethics committee and written informed consent.

Patients were characterized by having undergone surgery for coarctation of the aorta at the age of 9 ± 6.9 years (range 0.04–14.2 years) with the following techniques: Waldhausen repair (n = 2), resection with end-to-end anastomosis (n = 2), graft interposition (n = 1), and patch repair (n = 1). MR measurements in patients were performed 15.1 ± 6.3 (range 6.3–23.7) years after the intervention. Four patients presented a restenosis with 18.6% ± 8.2% (range 11–26%) stenosis grade. Five patients developed poststenotic dilatation with dilatation grade of 18.8% ± 14.2% (range 6–39%). Stenosis and dilatation grade are given relative to diameter of the distal descending aorta at the level of the diaphragm.

All measurements were performed on a 3 T system (Magnetom Trio, Siemens AG, Erlangen, Germany, standard eight-chanel phased-array coil). Patients received contrast agent (Gadobenate dimeglumine; Multihance®; Bracco, Milano, Italy) for contrast enhanced MR angiography of the aorta. In a 17-year-old patient, contrast agent was administered after written informed consent of the parents. In the US, the use of gadobenate dimeglumine in persons under 18 years of age is considered an off-label use.

Flow sensitive 4D PC-MRI data with three directional velocity encoding and covering the entire thoracic aorta were acquired using a navigator respiration controlled and ECG-gated radiofrequency-spoiled gradient echo sequence (15) (spatial resolution 1.9–2.4 × 1.7–1.8 × 2.0–2.5 mm^3, temporal resolution 39.2–40.8 ms, V_{enc} = 150–230 cm/s). Additional imaging parameters were adapted to the individual subject's anatomy and heart rate and ranged between: echo time = 2.48–2.53 ms, pulse repetition time = 4.9–5.2 ms, FOV = 213–255 × 320–340 mm, matrix 128–144 × 192, bandwidth 440 pixel/MHz, time frames per cardiac cycle = 14–23. Flip angles were independently adjusted for subgroups with and without contrast agents (α =15° and α =7°, respectively) to optimize image contrast. Data were acquired in a sagittal oblique 3D volume. The total scan time for the flow-sensitive measurement was 17.8 ± 4.9 min (heart-rate dependent range 9.5–30 min).

Echocardiography

Before MRI, patients underwent echocardiography per clinical standard procedure on a Vivid 7 system (General Electrics Vingmed Ultrasound, Horten, Norway) equipped with a 2.5–5 MHz phased-array transducer. CINE loops of three consecutive heart cycles were digitally stored for off-line analysis. Scans included measurements of velocities and diameters at the site of coarctation and/or repair in the most appropriate view.

Doppler values were recorded as maximum and mean velocity. Pressure gradients at the site of the aortic coarctation were derived from Doppler ultrasound using peak velocities and the simplified Bernoulli equation (see Eq. 3 below) for all six patients. During echocardiography the peak velocities were recoded by the operator but the full velocity-time curves were not available for retrospective analysis.

Data Analysis: Pressure Difference Estimation

Pressure gradients assuming a viscous, incompressible fluid were calculated using the Navier-Stokes equation

$$-\nabla p = \rho\left(\frac{\partial v}{\partial t} + v \cdot \nabla v - g\right) - \mu\nabla^2 v \qquad [1]$$

where p is the pressure, μ is the dynamic fluid viscosity, v is the measured three-directional velocity, ρ is the fluid density, and g is the gravitational force. The terms on the right-hand side represent from left to right: the transient inertia, the convective inertia, gravitational force, and viscous resistance. As phantom and human subjects were placed in a horizontal position in the scanner, the gravitational force was neglected for all calculations.

For a given voxel in the imaging volume, velocity values of the nearest temporal and spatial neighbors were used for calculation of a central difference as an approximation for temporal ($\frac{\partial v}{\partial t}$) and spatial first-order (∇v) and second-order ($\nabla^2 v$) velocity derivatives (8–10,19).

Based on derived pressure gradients, PDs $\Delta p(r,t)$ were calculated by iteratively solving the Poisson pressure equation using a similar approach as Tyszka et al. (9). The pressure is initialized by region growing integration of the pressure gradient with a user defined reference point ($\Delta p = 0$). Per iteration, the resulting PD in each voxel position r is refined as a weighted average of its current $\Delta p(r)$ and its expected $\Delta p'(r)$ estimated from the six nearest neighbor voxels. Relative change in the mean pressure in the entire volume of less than 0.1% between two successive iterations was set as convergence criterion. As data represent a real incompressible fluid the assumption was made that the flow obeys the divergence-free condition (e.g., incompressible) but this condition was not explicitly enforced (9).

All calculations were performed independently for each time frame. For in vivo pressure gradient estimation, blood properties were set to 3.2×10^{-3} Pa s and 1060 kg/m^3 for viscosity and density, respectively.

Data Analysis: Phantom Comparison

Phantom Measurement 1: Steady Flow

The pressure gradient Δp across the stenosis in the in vitro model was determined using velocities calculated from the known flow rate and phantom geometry using the modified Bernoulli equation

$$\Delta p = \frac{1}{2}\rho\left(v_2^2 - v_1^2\right) \qquad [2]$$

where v_1 and v_2 are velocities at locations proximal and at the maximum narrowing of the stenosis as illustrated in Fig. 1a. Additionally, the simplified Bernoulli equation was applied as used in clinical routine (5)

$$\Delta p = 4v_{\max}^2 \qquad [3]$$

where $v_{\max}$ represents the peak velocity at the maximum narrowing of the stenosis of the phantom (plane 2 in Fig. 1a).

To compare the results from Eqs. 2 and 3 with findings from Navier Stokes modeling (Eq. 1), the difference of the mean pressure gradient between two analysis planes was used to estimate the average pressure gradient (see Fig. 1a). The reference point ($\Delta p = 0$) was set directly in the stenosis at the site of the minimal diameter.

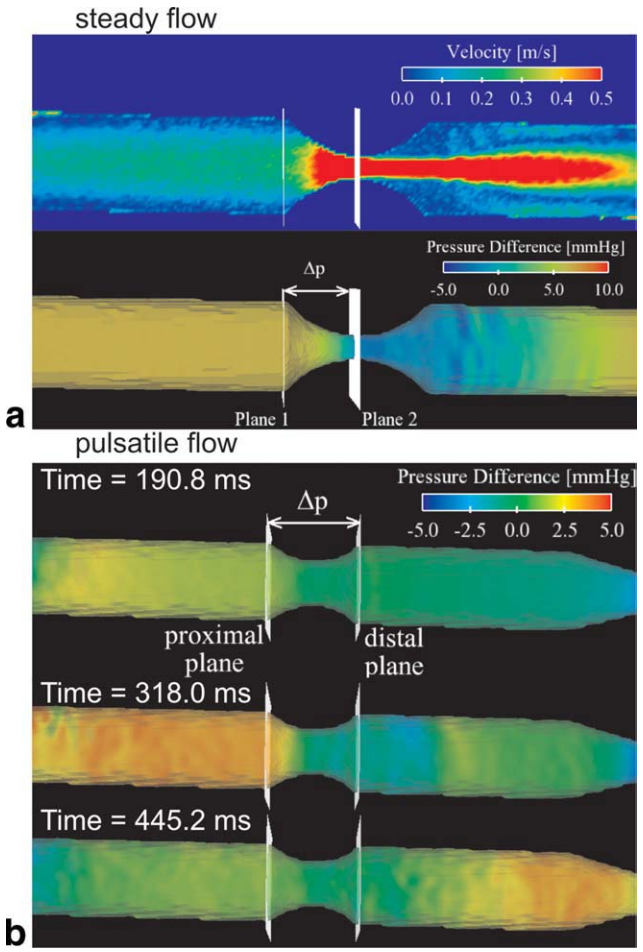

FIG. 1. **a**: Flow sensitive 4D MRI and pressure difference estimation in a stenosis model with constant flow (5.7 ± 0.5 L/min); Upper part: Measured velocity distribution in a central plane bisecting the phantom in longitudinal direction. Flow acceleration through the stenosis and the resulting velocity jet can clearly be appreciated. Lower part: Estimated pressure differences using the Navier Stokes equation and the measured three-directional velocities. The 3D distribution of the pressure difference was set to zero at the maximal narrowing (plane 2) and mapped onto a segmentation mask of the stenosis phantom. A marked pressure difference gradient (Δp) across the stenosis can clearly be appreciated. **b**: Pressure difference distribution along the stenosis model using pulsatile flow. Images capture three selected time frames of the flow cycle. Pressure inversion during diastole (time point 445.2 ms) can clearly be appreciated.

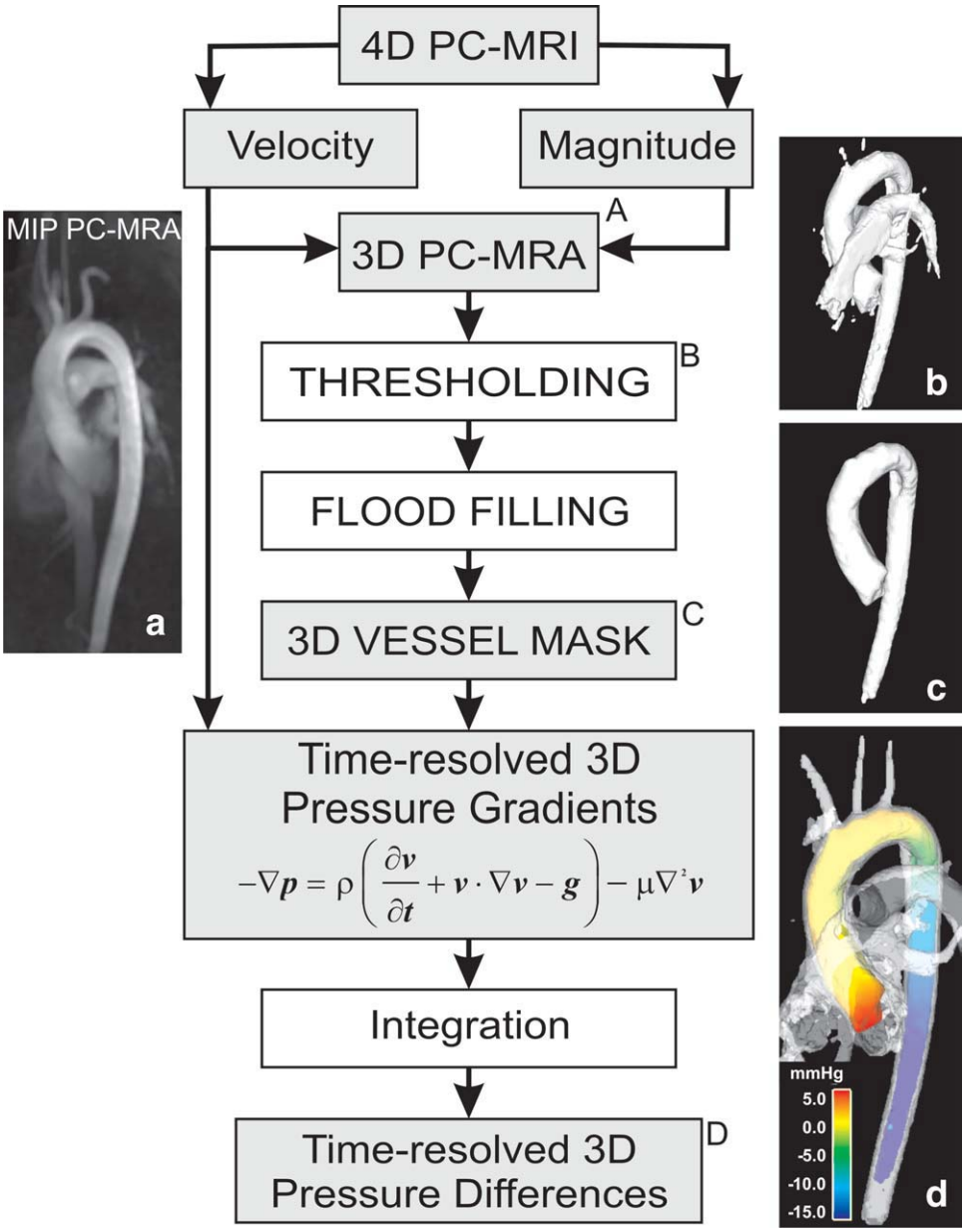

FIG. 2. Flow chart representing the necessary steps to calculate pressure difference maps for in vivo data. 3D visualization of the results (right column) shows the initial vessel mask after thresholding from the 3D PC-MRA data (top), application of the flood fill algorithms for aortic segmentation (mid) and the final systolic 3D pressured map inside the thoracic aorta (bottom).

Comparison of the different pressure calculations included error estimation. For velocities calculated according to Eqs. 2 and 3, the error was determined using gaussian error propagation based on uncertainties in flow rate (±8%, manufacturer specifications), pipe diameter (±6%, production tolerance), and stenosis diameter (±0.1%, production tolerance).

The MRI velocity noise was estimated using the standard deviation of the measured velocities during a flow-off measurement in the segmented in vitro model volume.

Phantom Measurement 2: Pulsatile Flow

3D pressured difference maps were calculated for each of 22 acquired time-frames using Navier-Stokes (Eq. 1). In addition, analysis planes located proximal and distal to the phantom stenosis (see Fig. 1b) were used to extract maximum velocities measured with MRI. These were used to determine time-resolved PDs, according to the modified (Eq. 2) and simplified (Eq. 3) Bernoulli equations. Calculated PD dynamics was compared with results from Navier Stokes modeling.

Data Analysis: In Vivo Data

The data analysis strategy is schematically summarized in Fig. 2. All represented processing steps were performed using home built software programmed in Matlab (The MathWorks, USA). To estimate the PDs in vivo, a reliable identification of the aortic lumen is required. Therefore, a time-averaged phase contrast MR angiography (PC-MRA) using the absolute velocity and magnitude weighting with additional noise masking and static tissue removal was calculated for each data set as described previously (20). For the calculation of pressure

gradients, the pulmonary system had to be separated from the aortic lumen. Therefore, simple thresholding of the 3D PC-MRA data was performed to create a three-dimensional binary mask. In some cases, morphological operations had to be applied to break the connectivity between the pulmonary system and the aorta and also to close holes in vessel segments.

To compare the data between subjects, a reference point (pressured difference $\Delta p = 0$) was set manually in the ascending aorta at the level of the lower edge of the pulmonary artery (see Fig. 4). This reference point was also used as a starting point for a 3D flood-filling algorithm to generate a 3D vessel mask containing only voxels from the aorta. All calculations regarding pressure gradients and differences were then restricted to the calculated aortic lumen.

For the 3D visualization of the resulting aortic geometry and the calculated PD maps, data were loaded into a commercial software package (EnSight, CEI, USA). The software could be used to manually position 2D analysis planes at any desired location in the 3D data volume. PD data in these analysis planes was exported and further analyzed using Matlab.

Data Analysis: Volunteers and Patients

For quantitative intersubject comparison of the in vivo data, five analysis planes were positioned at the anatomical land marks shown in Fig. 4: (1) directly above the reference point in the ascending aorta, (2) proximal to the first aortic branch, (3) distal to the last aortic branch, (4) at the level of reference point in the descending aorta (DAo I), and (5) 5 cm further downstream in the DAo (DAo II). Additionally, the results from our study were compared with literature values (9,10,13). For all analysis planes, the temporal evolution of the PDs averaged over the aortic lumen was calculated.

Comparison of systolic and diastolic peak PDs as well as time to peak values between healthy subjects and patients were performed for two anatomical positions (Last branch and DAo II as depicted in Fig. 4). Therefore, temporal interpolation of the PDs from original time resolution to 1 ms was performed.

Data Analysis: Aortic Coarctation

In data from patients, two additional analysis planes proximal and distal to the aortic coarctation were used for analysis of the PDs across the aortic narrowing (proximal and distal to the aortic coarctation, see Fig. 5). For all data, mean PDs relative to the reference point were calculated in each plane for all time frames. The time-resolved pressure gradient between two analysis planes was determined by calculating the difference of mean values from proximal and distal planes. Additionally, the maximum value of the pressure gradient was determined from all possible paths between the two analysis planes (21). The calculated pressure gradients across the coarctation were compared with findings from Doppler ultrasound and to MR-based PDs using the simplified Bernoulli method.

Statistics

Results are given as mean ± standard deviation if not stated otherwise. For comparison of peak and time-to-peak values between healthy subjects and patients, an unpaired *t*-test was performed using interpolated data. The correlation of pressure gradients calculated from MRI versus Doppler ultrasound was analyzed using linear regression analysis. Slope and intercept of linear regression were calculated. The overall quality of the regression was assessed using Pearson's correlation coefficient *r*; a correlation was considered significant for $P < 0.05$ (22).

RESULTS

In Vitro Data

Measurement 1

Figure 1 shows velocity (Fig. 1a, upper part) and PD (Fig. 1a, lower part) distribution along in the stenosis model. As steady flow was used for this measurement, the transient inertia (temporal acceleration) was not existent, thus PDs represent results of convective inertia and viscous resistance only.

Using velocities derived from the phantom geometry and flow rate, the modified and simplified Bernoulli approach revealed values of 8.2 ± 1.3 mmHg and 8.1 ± 1.3 mmHg, respectively. Pressure gradients calculated using PC-MRI velocities were 7.5 ± 0.1 mmHg, 7.5 ± 0.2 mmHg, and 7.4 ± 0.2 mmHg for modified and simplified Bernoulli equations and Navier-Stokes approach, respectively. The results show good agreement between the different approaches and error calculations revealed low uncertainties.

Measurement 2

Figure 1b illustrates PD distribution along the stenosis model for three selected time frames of the pulsatile flow cycle. In this pulsatile flow measurement, one can observe both the influence of the transient and convective acceleration terms in the Navier-Stokes pressure modeling. As for the steady-flow condition, convective acceleration (spatially changing velocities) results in a pressure gradient across the stenosis. Transient acceleration (temporally changing velocities) resulted in a pressure inversion during diastole (time 445.2 ms) compared with the situation in systole. This pressure inversion is associated with deceleration of blood flow in diastole as well as with the pressure pulse wave reflection at the periphery (14,23). The dynamics changes of PDs between the two analysis planes in Fig. 1b during one flow cycle are shown in Fig. 3. Time-resolved PDs across the stenosis show good agreement between Navier Stokes modeling and the reference methods (Bernoulli). Linear regression analysis results are: $y = 1.17x + 0.40$, $r = 0.95$, and $P < 0.05$ for modified Bernoulli vs. Navier-Stokes modeling; and $y = 0.85x + 0.25$, $r = 0.97$, and $P < 0.05$ for simplified Bernoulli versus Navier-Stokes.

In Vivo Data

The cumulative results for all 12 normal subjects and 6 patients are summarized in Fig. 4. The graphs represent

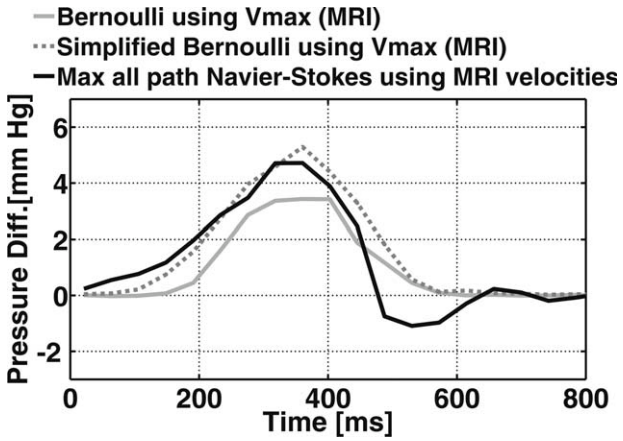

FIG. 3. The curves represent time resolved pressure gradient over the stenosis in the model. Maximum velocity measured in MRI was used to calculate pressure differences with modified Bernoulli (gray solid line) and simplified Bernoulli (gray dotted line) equations. The black line represents pressure differences calculated as maximum over all paths using the Navier-Stokes equation.

PDs averaged over all 12 volunteers (solid lines, mean ± interindividual standard deviation) and 6 patients (dashed lines, interindividual standard deviation not shown for better visibility of the results) for five analysis planes. High systolic PDs as well as the expected inverted PDs during early diastole (9) can be appreciated. The small standard deviations for healthy subjects indicate high data consistency.

In patients, PD-time curves were of similar shape but demonstrated higher peak PDs and delayed times-to-peak. The descriptive statistics of peak and time-to-peak pressure gradients for volunteers and patients is summarized in Table 1. Comparison of peak and time to peak values between healthy subjects and patients using unpaired *t*-test revealed no statistically significant differences for peak diastolic and time to peak systolic PDs at the "Last Branch" location (see Fig. 4). All other values showed statistically significantly increased peak and time-to-peak PDs in coarctation patients compared with healthy controls.

In patients, peak pressure gradients across the aortic coarctation (Fig. 5) were compared between the reference standard echocardiography and MRI findings at the same location (Fig. 6). The example in Fig. 5 illustrates that simplified Bernoulli calculations (top right, orange curve) resulted in a different temporal evolution of maximum PD across the coarctation compared with Navier Stokes modeling (top right, white curve). Navier stokes provided improved peak pressure estimation compared to echocardiography and could show diastolic pressure inversion across the stenosis, which could not be reproduced with the simplified assumptions of the Bernoulli approach.

In all subjects, MRI-based peak mean pressure gradients underestimated the pressure gradient compared with echocardiography by 60.1 ± 17.8% and did not shown a significant correlation with echocardiography. Pressure gradients calculated using the simplified Bernoulli method where maximum velocity was measured

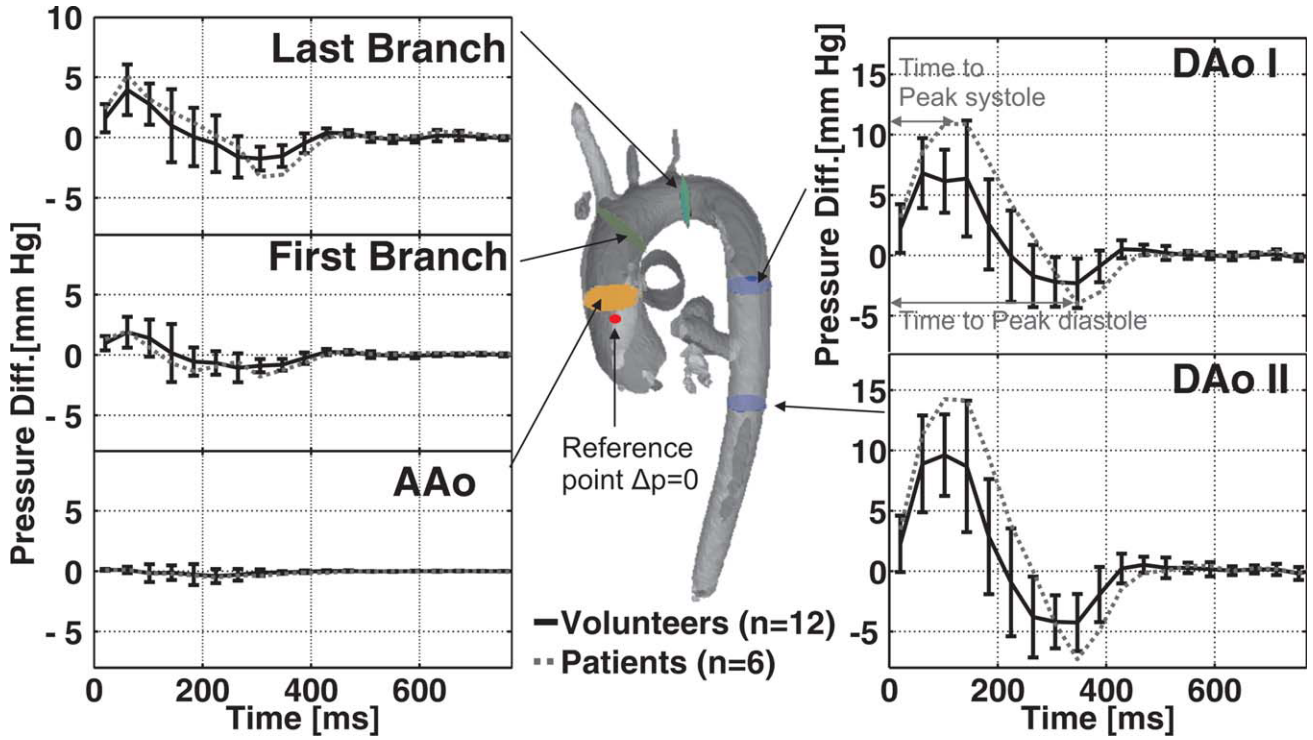

FIG. 4. Time-resolved pressure differences in five analysis planes relative to the reference point ($\Delta p = 0$) averaged over 12 volunteers (solid black line) and over six patients with coarctation (dotted gray line). Standard deviations in volunteers represent intersubject variations. Standard deviations in patients are omitted due to visibility reasons. [Color figure can be viewed in the online issue, which is available at wileyonlinelibrary.com.]

Table 1
Comparison of Peak and Time to Peak Pressure Differences (PDs) Between Healthy Subjects and Patients for Two Anatomical Positions (Last Branch and DAo II as Depicted in Fig. 4)

		Peak systolic PD (mmHg)	Time to peak systolic PD (ms)	Peak diastolic PD (mmHg)	Time to peak diastolic PD (ms)
Last Branch	Healthy subjects	4.7 ± 1.8 (3.2–9.5)	54.8 ± 27.1 (21–117)	−2.9 ± 1.7 (−1.1 to −6.6)	269.5 ± 69.7 (122–359)
	Patients	9.6 ± 5.0 (1.5–15.5)	89.3 ± 73.3 (22–203)	−6.1 ± 4.4 (−0.5 to −10)	319.2 ± 33 (286–362)
	t-test	$P < 0.05$	NS	NS	$P < 0.05$
DAo II	Healthy subjects	12.5 ± 2.9 (8.5–17.9)	89.7 ± 33.6 (36–124)	−6.0 ± 2.0 (−3.4 to −10.0)	291.5 ± 45.6 (208–368)
	Patients	24.7 ± 13.8 (11.1–50.7)	134.3 ± 37.6 (81–194)	−11.6 ± 4.2 (−5.3 to 16.8)	323.8 ± 21.0 (295–351)
	t-test	$P < 0.05$	$P < 0.05$	$P < 0.05$	$P < 0.05$

Note that values for "Last Brach" were measured directly distal to the branching point of the left subclavian artery and thus proximal to the aortic coarctation. Values are given as mean ± standard deviation with the minimum–maximum range in brackets. NS, not significant.

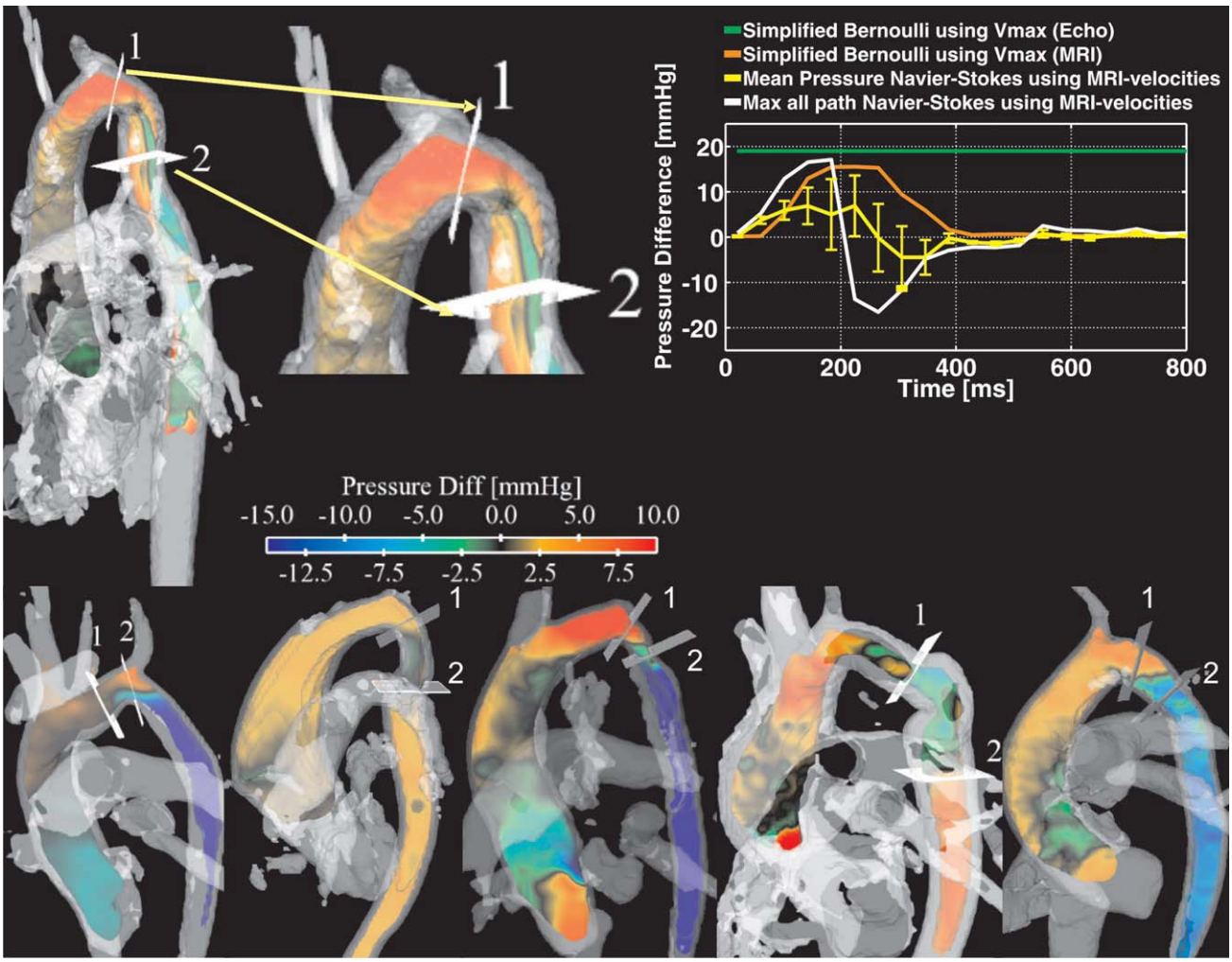

FIG. 5. 4D pressure difference mapping in six patients with aortic coarctation. The upper part illustrates the analysis strategy for patient 2. Upper left: 3D systolic pressure differences directly mapped onto the aorta; upper right: yellow curve: time-resolved mean pressure gradient between planes 1 and 2 calculated from MR data using Navier-Stokes modeling; white curve: time-resolved peak pressure gradient calculated from MR data using Navier-Stokes modeling; orange curve: time-resolved pressure gradient value calculated using simplified Bernoulli equation with peak velocity measured in MRI; green curve: pressure gradient measured using echocardiography. Lower part: Examples for all other 5 patients (1 and 3–6), showing 3D pressure differences directly mapped onto the aorta during systole.

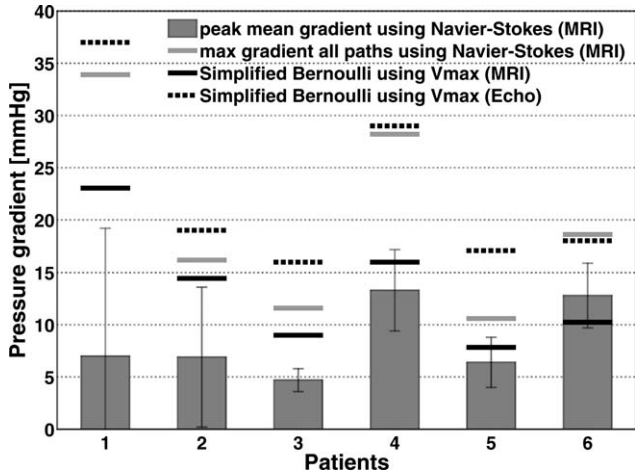

FIG. 6. Comparison of peak pressure gradients across aortic coarctation measured in echocardiography (black dotted line) and calculated from MRI data using simplified Bernoulli equation (black solid line), the Navier-Stokes equation (gray bars, peak mean difference between analysis planes ± standard deviation), and as maximum of all possible paths between planes 1 and 2 in Fig. 5 (gray solid line).

in MRI also demonstrated an underestimation of 41.3 ± 9.9% but significantly correlated with pressure gradients determined by in echocardiography ($r = 0.94$, $P < 0.05$). Considerably improved performance was found for MR pressure gradients determined from all possible paths between analysis planes 1 and 2 (underestimation 14.7 ± 15.5%) also reflected by excellent correlation with echocardiography ($r = 0.96$, $P < 0.05$).

DISCUSSION

The results of our in vitro and in vivo studies demonstrate the potential of 4D pressure gradient mapping based on flow-sensitive 4D MRI data. The advantage of the presented method is related to the possibility to derive time-resolved three-dimensional PDs. The complete spatial and temporal coverage may help to evaluate the impact of local pathologies (stenosis) on regional and global pressure gradient alterations in the entire system over time. Furthermore, one can combine pressure gradient data with additional information from flow-sensitive 4D PC-MRI such as flow visualization (vector fields, streamlines, and particle traces), flow quantification and derived wall parameters (wall shear stress, etc.). Such combination of multiple parameters may provide new insights in the development of secondary pathologies (e.g., poststenotic aneurysms) as illustrated in Fig. 7.

In this study, comparison based on a stenosis model and constant flow showed good agreement between different approaches using Navier-Stokes, the modified Bernoulli and simplified Bernoulli equation. Further, the investigation of a stenosis model using pulsatile flow demonstrated the intrinsic consistency of the MRI data.

However, no additional measurements using another modality were performed to obtain an independent measure of the pulsatile flow waveform inside the phantom. It was thus not possible to calculate the expected pressure based on the flow curve and known geometry. Nevertheless, the presented comparisons between PDs using Navier Stokes modeling with standard methods (Bernoulli) for pulsatile flow indicates the intrinsic consistency of the presented data analysis strategy.

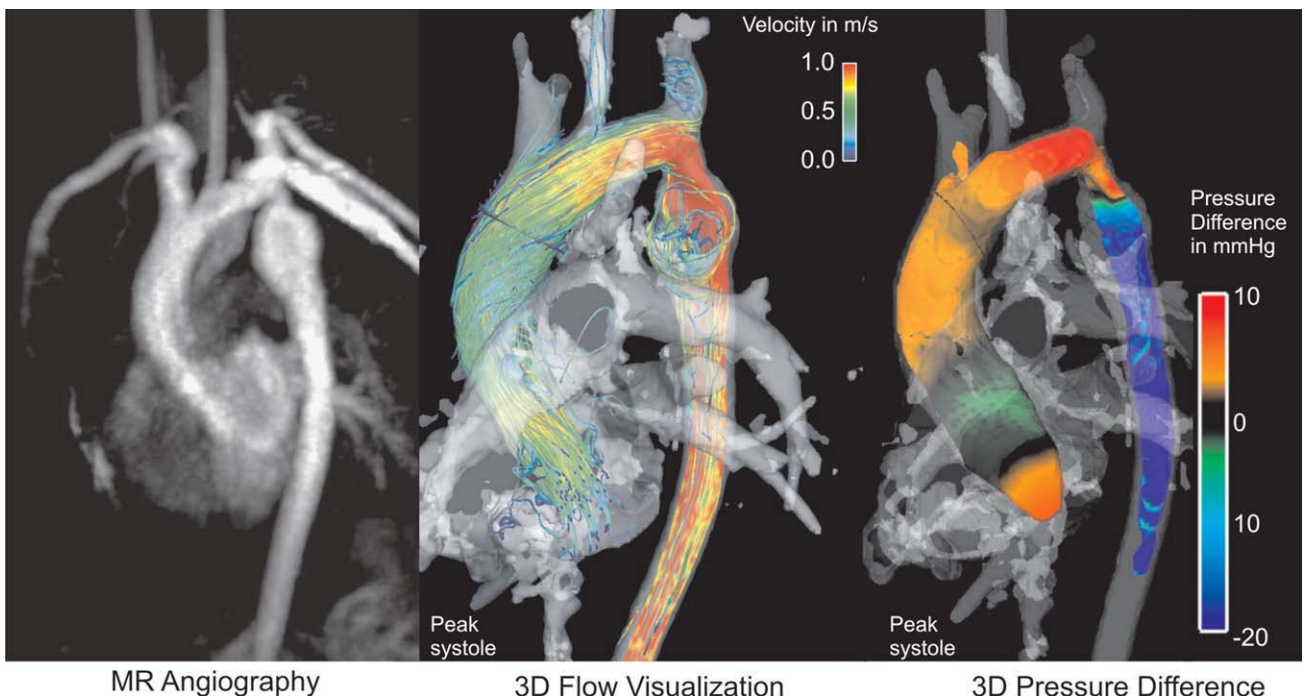

FIG. 7. Combined visualization of aortic geometry by MR angiography, systolic blood flow, and 3D pressure differences in a patient with aortic coarctation.

The in vivo study demonstrated that time-averaged aortic vessel geometry derived from flow sensitive 4D PC-MRI data can be successfully used in parallel with the acquired velocity field to semi-automatically determine time-resolved pressure gradients and 4D PDs maps.

PDs found in our cohort were in good to moderate agreement with findings in other MRI studies (9,10,13). In the study by Tyszka et al. maximum/minimum PDs between positions ascending aorta and DAo II were 11/−5 mmHg compared with 7/−3 mmHg in our study. Between first and last supra-aortic branches PDs in the study by Ebbers et al. were 3/−2 mmHg, in the study by Nagao et al. 1/−0.6 mm Hg compared with 2/−1 mmHg in our study. Nagao et al. reported PDs of 0.6/−0.4 mmHg between the ascending aorta and the first supra-aortic branch. In our study, we measured 1.9/−0.8 mmHg. Note that the results from our study reflect average values over 12 healthy subjects while in all other studies only one subject was examined, which limits the power of a statistical comparison.

In a study using pressure catheters, Mills et al. determined time-resolved pressure waves at certain positions in the aorta (24). Between the ascending and descending aorta the difference of peak pressures was ~8 mmHg. In our study, we found 7 mmHg between approximately the same positions. To our knowledge, to date no other data on spatially resolved and temporally resolved aortic relative PDs in healthy subjects are available that could be used to compare our results to standard methods such as those by echocardiography or catheter measurements.

The applied approach for vessel segmentation can only identify the inner part of the aortic lumen and does not provide the exact location of aortic walls due to the applied morphological operations. As a result, not all measured velocity values are included in the calculation of the relative PDs. Nevertheless, the time-resolved 3D PDs inside the determined lumen could still be reliably estimated from volunteer data as indicated by the consistency of the results (i.e., low interindividual variations).

Additionally, the divergence-free condition was not explicitly enforced in the data. However, it was shown that measured velocity field is not completely divergence-free due to imaging noise and partial volume effects within the moving fluid, so the PD calculation could benefit from achieving the divergence-free condition (9,25,26).

In patients, the pressure gradients were underestimated compared with echocardiography, which could be explained by the lower spatial and temporal resolution in MRI resulting in partial volume effects and temporal filtering and thus underestimation of peak velocities. Also, turbulence or complex flow resulting in signal dephasing could further compromise the accuracy of pressure gradient estimation from PC-MRI (27). Nevertheless, the maximum pressure gradient of all possible paths within the pathology calculated from MRI velocity data are in good agreement with echocardiography.

However, echocardiography could also have overestimated the pressure gradients. Several studies have reported a close correlation ($r > 0.76$) between Doppler-estimated and catheterization-determined pressure gradient with a systematic overestimation on the part of echocardiography (28,29), especially in the setting when the proximal velocities exceed 1 m/s or when gradients across the stenosis are low (28). In mild vessel stenosis [peak Doppler gradient < 20 mmHg (30)], measurement of instantaneous pressure drop by Doppler overestimates the pressure gradient because the velocity proximal to the obstruction is relatively higher to the distal velocity (31). The patients of our population showed relative small velocity changes (34% ± 28% using MRI velocities) across the stenotic area, such that proximal velocity and viscous effects have a greater importance than in patients with higher velocity changes. As velocities are acquired in a window placed in the center of the vessel, echocardiography acquisitions are prone to overestimating velocities, thereby potentially overestimating Δp to an even higher degree (Eq. 3). Applying the Navier-Stokes approach in patients with mild stenosis may thus help to overcome this overestimation by simplified Bernoulli, as proximal and distal velocities as well as viscous effects are accounted for.

Furthermore, the anatomy of the aortic vessel and the shape of the jet-stream have an important impact on the detected flow velocity (29). Eccentric jet, often seen in coarctation, additionally leads to overestimation when using the simplified Bernoulli approach (32). Because of complete temporal and spatial coverage in MRI data, it is possible to overcome these limitations and observe pressure development over long distances without being influenced by vessel shape and jet stream location in the stenosis. Furthermore, the presented Navier-Stokes approach could also be applied to regions that cannot be examined with echocardiography. A disadvantage compared with the routinely used Bernoulli method is the long acquisition and computation time. Nevertheless, the Navier-Stokes method was rarely used to date and provides new information (time-resolved 3D pressure maps with volumetric coverage) and future studies are needed to evaluate potential benefits associated with this new information.

A shortcoming of this study setup is that no pressure catheter measurements were available for the patients, which would constitute the most reliable reference method and could help overcoming limitations of the ultrasound. After there herein presented validation and feasibility data, future studies will include patients with catheter-based invasive pressure measurements as the standard of reference. Furthermore, results presented here for analysis of peak systolic PD and time-to-peak systolic PD revealed significant differences for all parameters determined in a plane distal to the pathology. In the plane proximal to the stenosis, higher systolic PDs and later occurrence of the diastolic peak were of statistical significance. However, these results were determined in a small cohort of patients and further investigations are needed including a larger number of patients.

It is important to note that the iterative approach used in this study was limited by lengthy computation times and pressure gradient underestimation. In a recent study, Ebbers et al. presented a multigrid-based solver for the pressure Poisson equation, which provided faster and better estimates of the relative pressure fields from velocity MRI data compared with the iterative approaches

(14). In this study, we did not compare the iterative approach with the method introduced by Ebbers and Farneback (14). However, further studies should involve comparisons of both techniques in a large cohort of subjects.

In addition, the pressure gradient estimation required the derivation of local temporal and convective acceleration by calculating spatial and temporal derivatives of the measured time-resolved velocity vector field. The calculation of derived quantities results in noise amplification of the underlying measured data (velocities), and those can corrupt the final pressure gradients. To reduce noise and improving accuracy of the derived quantities, directly acquired acceleration fields with recently reported fast 3D acceleration encoded PC-MRI (33) may help as has been shown in previous studies (19,34). Finally, in this pilot study, the time-averaged calculation of vessel boundaries was implemented; however, future studies may benefit from time-resolved vessel segmentation, which may improve the calculation of pressure gradients.

In conclusion, this study demonstrates the potential of the applied approach to derive 4D pressure gradients from time-resolved 3D PC-MRI. In addition to encouraging phantom comparison results, in vivo MRI-derived pressure gradients showed good correlation with moderate underestimation compared with the available clinical standard Doppler ultrasound. As such differences could have been influenced by a relative overestimation of ultrasound and the iterative approach to pressure gradient calculation, future studies need to focus on a comparison with direct invasive measurements.

REFERENCES

1. Currie PJ, Seward JB, Reeder GS, Vlietstra RE, Bresnahan DR, Bresnahan JF, Smith HC, Hagler DJ, Tajik AJ. Continuous-wave Doppler echocardiographic assessment of severity of calcific aortic stenosis: a simultaneous Doppler-catheter correlative study in 100 adult patients. Circulation 1985;71:1162–1169.
2. Cohn JN, Quyyumi AA, Hollenberg NK, Jamerson KA. Surrogate markers for cardiovascular disease: functional markers. Circulation 2004;109 (Suppl. 1):IV-31–46.
3. Walder LA, Schaller FA. Diagnostic cardiac catheterization. When is it appropriate? Postgrad Med 1995;97:37–42, 45.
4. Skinner JS, Adams PC. Outpatient cardiac catheterisation. Int J Cardiol 1996;53:209–219.
5. Hatle L, Brubakk A, Tromsdal A, Angelsen B. Noninvasive assessment of pressure drop in mitral stenosis by Doppler ultrasound. Br Heart J 1978;40:131–140.
6. Hatle L, Angelsen B. Doppler Ultrasound in cardiology: physical principles and clinical applications. Philadelphia: Lea and Febiger; 1982. 89 p.
7. Oshinski JN, Parks WJ, Markou CP, Bergman HL, Larson BE, Ku DN, Mukundan S, Jr, Pettigrew RI. Improved measurement of pressure gradients in aortic coarctation by magnetic resonance imaging. J Am Coll Cardiol 1996;28:1818–1826.
8. Yang GZ, Kilner PJ, Wood NB, Underwood SR, Firmin DN. Computation of flow pressure fields from magnetic resonance velocity mapping. Magn Reson Med 1996;36:520–526.
9. Tyszka JM, Laidlaw DH, Asa JW, Silverman JM. Three-dimensional, time-resolved (4D) relative pressure mapping using magnetic resonance imaging. J Magn Reson Imaging 2000;12:321–329.
10. Ebbers T, Wigstrom L, Bolger AF, Engvall J, Karlsson M. Estimation of relative cardiovascular pressures using time-resolved three-dimensional phase contrast MRI. Magn Reson Med 2001;45:872–879.
11. Lum DP, Johnson KM, Paul RK, Turk AS, Consigny DW, Grinde JR, Mistretta CA, Grist TM. Transstenotic pressure gradients: measurement in swine—retrospectively ECG-gated 3D phase-contrast MR angiography versus endovascular pressure-sensing guidewires. Radiology 2007;245:751–760.
12. Moftakhar R, Aagaard-Kienitz B, Johnson K, Turski PA, Turk AS, Niemann DB, Consigny D, Grinde J, Wieben O, Mistretta CA. Noninvasive measurement of intra-aneurysmal pressure and flow pattern using phase contrast with vastly undersampled isotropic projection imaging. AJNR 2007;28:1710–1714.
13. Nagao T, Yoshida K, Okada K, Miyazaki S, Ueguchi T, Murase K. Development of a noninvasive method to measure intravascular and intracardiac pressure differences using magnetic resonance imaging. Magn Reson Med Sci 2008;7:113–122.
14. Ebbers T, Farneback G. Improving computation of cardiovascular relative pressure fields from velocity MRI. J Magn Reson Imaging 2009; 30:54–61.
15. Markl M, Harloff A, Bley TA, Zaitsev M, Jung B, Weigang E, Langer M, Hennig J, Frydrychowicz A. Time-resolved 3D MR velocity mapping at 3T: improved navigator-gated assessment of vascular anatomy and blood flow. J Magn Reson Imaging 2007;25:824–831.
16. Holton AD, Walsh EG, Brott BC, Venugopalan R, Hershey B, Ito Y, Shih A, Koomullil R, Anayiotos AS. Evaluation of in-stent stenosis by magnetic resonance phase-velocity mapping in nickel-titanium stents. J Magn Reson Imaging 2005;22:248–257.
17. Chernobelsky A, Shubayev O, Comeau CR, Wolff SD. Baseline correction of phase contrast images improves quantification of blood flow in the great vessels. J Cardiovasc Magn Reson 2007;9:681–685.
18. Lorenz R, Benk C, Bock J, Korvink J, Markl M. Improved simulation of 3D flow characteristics in a pressure controlled in vitro model system. In: Proceedings of 18th Annual Meeting of ISMRM, Stockholm, Sweden, 2010. 3711.
19. Balleux-Buyens F, Jolivet O, Bittoun J, Herment A. Velocity encoding versus acceleration encoding for pressure gradient estimation in MR haemodynamic studies. Phys Med Biol 2006;51:4747–4758.
20. Bock J, Frydrychowicz A, Stalder AF, Bley TA, Burkhardt H, Hennig J, Markl M. 4D phase contrast MRI at 3 T: effect of standard and blood-pool contrast agents on SNR, PC-MRA, and blood flow visualization. Magn Reson Med 2010;63:330–338.
21. Sondergaard L, Stahlberg F, Thomsen C, Stensgaard A, Lindvig K, Henriksen O. Accuracy and precision of MR velocity mapping in measurement of stenotic cross-sectional area, flow rate, and pressure gradient. J Magn Reson Imaging 1993;3:433–437.
22. Rodgers JL, Nicewander WA. Thirteen ways to look at the correlation coefficient. Am Stat 1988;42:59–66.
23. McDonald DA. The relation of pulsatile pressure to flow in arteries. J Physiol 1955;127:533–552.
24. Mills CJ, Gabe IT, Gault JH, Mason DT, Ross J, Jr, Braunwald E, Shillingford JP. Pressure-flow relationships and vascular impedance in man. Cardiovasc Res 1970;4:405–417.
25. Buonocore MH. Algorithms for improving calculated streamlines in 3-D phase contrast angiography. Magn Reson Med 1994;31:22–30.
26. Skrinjar O, Bistoquet A, Oshinski J, Sundareswaran K, Frakes D, Yoganathan A. A divergence-free vector field model for imaging applications. International Symposium on Biomedical Imaging: From Nano to Macro, Boston, USA 2009. pp 891–894.
27. Nasiraei-Moghaddam A, Behrens G, Fatouraee N, Agarwal R, Choi ET, Amini AA. Factors affecting the accuracy of pressure measurements in vascular stenoses from phase-contrast MRI. Magn Reson Med 2004;52:300–309.
28. Marx GR, Allen HD. Accuracy and pitfalls of Doppler evaluation of the pressure gradient in aortic coarctation. J Am Coll Cardiol 1986;7: 1379–1385.
29. Rao PS, Carey P. Doppler ultrasound in the prediction of pressure gradients across aortic coarctation. Am Heart J 1989;118:299–307.
30. Fyler DC, Keane JF, Lock JE. Nadas' pediatric cardiology. Philadelphia. Hanley & Belfus: Hanley & Belfus; 1992.
31. Colan SD. Quantitative applications of Doppler cardiography in congenital heart disease. Cardiovasc Interv Radiol 1987;10:332–347.
32. Lai W. Echocardiography in pediatric and congenital heart disease: from fetus to adult. Wiley-Blackwell; 2009.
33. Staehle F, Bauer S, Jung B, Hennig J, Markl M. 3-Directional Fast Acceleration Encoding. In Proceedings of 17th Annual Meeting of ISMRM, Honolulu, USA 2009 (Abstract 2665).
34. Tasu JP, Mousseaux E, Delouche A, Oddou C, Jolivet O, Bittoun J. Estimation of pressure gradients in pulsatile flow from magnetic resonance acceleration measurements. Magn Reson Med 2000;44:66–72.